Alternating-Current Impedance and Chronoamperometry Studies of Poly(vinylidene fluoride-*co*-hexafluoropropylene)–Polyacrylonitrile-Based Microporous Polymer Blend Electrolytes Prepared by a Phase-Inversion Technique

N. T. Kalyana Sundaram, T. Vasudevan, A. Subramania

Advanced Materials Research Lab, Department of Industrial Chemistry, Alagappa University, Karaikudi 630 003, India

Received 6 June 2006; accepted 28 September 2006
DOI 10.1002/app.26355
Published online 16 May 2007 in Wiley InterScience (www.interscience.wiley.com).

ABSTRACT: This article describes a comparative study of poly(vinylidene fluoride-*co*-hexafluoropropylene)–polyacrylonitrile-based plain gel polymer blend electrolytes and microporous gel polymer blend electrolytes. Scanning electron microscopy, differential scanning calorimetry, alternating-current impedance, chronoamperometry, and dielectric spectroscopy studies were carried out. The microporous gel polymer blend electrolytes enhanced the ionic conductivity, lithium transference number, and dielectric permittivity, and this could be attributed to a higher uptake of the electrolyte solution (an increase in the number of charge carriers) by the porous structure. The temperature dependence of the ionic conductivity of the polymer electrolyte followed an Arrhenius relationship. An LSV experiment was carried out to investigate the electrochemical stability in the polymer electrolyte. Finally, charge–discharge studies of lithium-ion cells made from the coupling of gel polymer blend electrolytes (plain and microporous) with $LiMg_{0.10}Mn_{1.90}O_4$ as a cathode and carbon as an anode were conducted. © 2007 Wiley Periodicals, Inc. J Appl Polym Sci 105: 2830–2836, 2007

Key words: electrochemistry; gels

INTRODUCTION

Solid-state lithium-ion polymer batteries may be one of the best choices for electrochemical power sources of the future, being characterized by high energy density, low weight, reliability, safety, and excellent cycle performance.[1–3] For instance, in 1997 alone, worldwide sales of rechargeable lithium-ion polymer batteries exceeded 1.6 billion dollars.[4] Because of government mandates for electric vehicles and the ever-increasing demand for portable power sources, the production of rechargeable lithium-ion batteries is expected to grow more than 20% per year.[5,6] However, several factors in lithium-ion batteries, especially in the electrolyte, have limited commercial usage. Most lithium-ion batteries use a liquid electrolyte, which requires the use of a microporous polymer electrolyte to separate the electrodes.[7–9] These microporous polymer electrolytes must possess electrochemical properties comparable to liquid electrolytes, such as a high ionic conductivity and lithium transference number. The technological impact of developing an electrolyte that improves the ionic conductivity and mechanical strength is significant. Usually, good mechanical stability and high ionic conductivity for a polymer electrolyte exhibit a contradictory relationship: the higher the ionic conductivity is of a polymer electrolyte film, the lower its mechanical stability is. Until now, for all solid-state lithium batteries, poly(vinylidene fluoride-*co*-hexafluoropropylene) (PVdF-*co*-HFP) has been considered one of the most promising candidates because of its favorable ionic conductivity, good mechanical strength, and acceptable cost.[10–12] At an ambient temperature, the PVdF-*co*-HFP polymer electrolyte exhibits acceptable mechanical strength. However, the PVdF-*co*-HFP polymer electrolyte shows practical ionic conductivity only at temperatures higher than the melting point, and at such high temperatures, it exists in a quasiliquid state and becomes very flexible and therefore shows very poor mechanical strength. A weak polymer electrolyte film easily causes a short circuit between a cathode and an anode when it is applied to all solid-state lithium-ion batteries. Therefore, it is still an attractive research topic to develop mechanically stable polymer electrolytes with high ionic conductivity, especially at room temperature.

Many kinds of polymers, such as polyacrylonitrile (PAN) and poly(methyl methacrylate), have been

Correspondence to: A. Subramania (drasubramania@yahoo.co.in).

Contract grant sponsor: DST (New Delhi, India).

used as a second phase for polymer electrolytes to obtain gel polymer blend electrolytes.[13,14] The addition of a second-phase polymer has been proved to be an effective approach to improve the overall performance of polymer blend electrolytes because polymer blend electrolytes exhibit fully amorphous features and show favorable ionic conductivity and good mechanical strength at ambient temperatures.

Generally, various techniques such as the template-imprinting technique (sol–gel processing)[15] and immersion precipitation technique[16,17] have been used to prepare microporous polymer membranes. The drawback of a microporous polymer film prepared with this technique is a smaller pore volume and pore size (ca. 30 nm). However, these methods are inconvenient because they increase the cost of the process and present safety concerns related to the handling of large volumes of volatile solvents.[19] These polymers, therefore, cannot absorb sufficient amounts of an electrolyte solution to achieve high ionic conductivity at an ambient temperature. To overcome this shortcoming, the phase-inversion technique, for which a microporous polymer matrix can be prepared through the casting of a polymer solution and the evaporation of the solvent and nonsolvent in turn, has been developed and used successfully to prepare microporous polymer membranes.[20–25]

In this work, we present the results of a comparative study of PVdF-*co*-HFP–PAN-based plain gel polymer blend electrolytes (PGPBEs) and microporous gel polymer blend electrolytes (MPGPBEs) and explain how the porosity of the membranes affects the ionic conductivity, lithium transference number, dielectric permittivity, specific capacity, and cycle performance when they are used as separators in lithium-ion batteries.

EXPERIMENTAL

Materials

PVdF-*co*-HFP with an average molecular weight greater than 5,00,000 (Aldrich), PAN with an average molecular weight greater than 1,00,000 (Aldrich), and $LiClO_4$ and $LiAsF_6$ (E-Merck, Germany) were dried in a vacuum oven at 80°C under 10^{-3} Torr of pressure for 48 h. Ethylene carbonate (EC) and diethyl carbonate (DEC; Acros Organic, Belgium) were purified by distillation under reduced pressure.

Preparation of a polymer blend of an optimized composition

Different compositions of PVdF-*co*-HFP and PAN were dissolved in DMF. The resultant viscous solutions were spread as films on a glass substrate with a doctor's blade. Finally, the films were dried at 80°C in a vacuum oven under 10^{-3} Torr of pressure for 3 h to remove any further traces of DMF. The thickness of the films was in the range of 150–200 μm. Then, the polymer blend films were soaked in 1*M* $LiClO_4$ in EC–DEC (1 : 1 v/v ratio) for 18 h to get PGPBEs. The ionic conductivity and film strength were measured to optimize the required polymer blend ratio.

Preparation of an MPGPBE

An optimized ratio of the PVdF-*co*-HFP–PAN-based microporous polymer blend membrane was obtained by the phase-inversion technique as described elsewhere.[26,27] The membrane was finally soaked in 1*M* $LiClO_4$ in EC/DEC (1 : 1 v/v ratio) for 18 h to get the MPGPBE.

Characterization

Scanning electron microscopy (SEM) studies were carried out with a JEOL JSM-35CF scanning electron microscope to determine the surface morphology of PVdF-*co*-HFP–PAN-based polymer blend film/membranes. The porosity (P) was determined through the weighing of the sample with and without 1-butanol and with eq. (1):[28]

$$P = (m_a/\rho_a)/(m_a/\rho_a + m_p/\rho_p) \quad (1)$$

where m_a is the film weight after impregnation with 1-butanol; m_p is the dried film weight; and ρ_a and ρ_p are the densities of the 1-butanol and dried film, respectively.

The extent of swelling (S_w) of the polymer blend film/membranes was determined with eq. (2):[29]

$$S_w = (W - W_0)/W_0 \times 100 \quad (2)$$

where W_0 is the weight of the dried membrane and W is the weight of the swollen membrane.

The thermal behavior of the gel polymer blend electrolytes was studied with a Dupont TA 2000 differential scanning calorimeter. Each sample was scanned from −100 to 200°C through heating at a scanning rate of 1°C/min under a nitrogen atmosphere.

Conductivity measurements were performed by the sandwiching of the polymer blend electrolyte between two stainless steel (SS) electrodes with a Hioki 3522-50 LCR meter over a frequency range of 1 mHz to 100 kHz at a scanning rate of 1 mV/s with various temperatures ranging from 298 to 353 K.

The electrochemical stability of MPGPBE was evaluated with a cell featuring an SS working electrode and lithium as counter and reference electrodes through linear sweep voltammetry at 25°C. A direct-current polarization cell was constructed by the

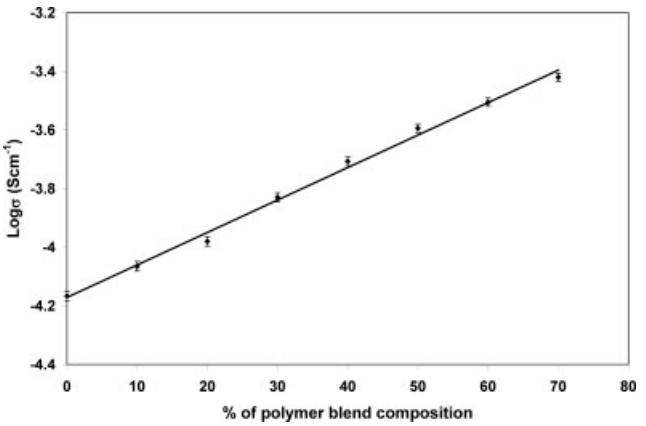

Figure 1 Polymer blend composition (wt %) versus the ionic conductivity (σ) of PVdF-*co*-HFP–PAN–1*M* $LiClO_4$–EC–DEC.

sandwiching of the gel polymer blend electrolyte between symmetrical lithium metal electrodes, and the experiment was performed as described previously[9] to determine the lithium transference number of the gel polymer blend electrolytes. These cells were assembled in a drybox under an argon atmosphere.

The frequency dependence of the dielectric permittivity was determined by the sandwiching of the gel polymer blend electrolyte between two SS electrodes with a Hioki model 3532 LCR meter over a frequency range of 40 Hz to 5 MHz at room temperature.

Carbon and $LiMg_{0.10}Mn_{1.90}O_4$ were employed as negative and positive electrodes, respectively. The laminated cell, which consisted of carbon, the gel polymer blend electrolyte, and $LiMg_{0.10}Mn_{1.90}O_4$, was assembled in a drybox under an argon atmosphere, and the charge–discharge studies were performed at a C/10 rate with cutoff voltages of 4.8 and 3.0 V for the upper and lower limits, respectively, to prevent the decomposition of electrolytes.

RESULTS AND DISCUSSION

The ionic conductivity of PVdF-*co*-HFP–PAN-based PGPBEs was measured through the variation of the proportionate ratio, as shown in Figure 1. An increase in the PAN content in the PVdF-*co*-HFP matrix increases the ionic conductivity and decreases the dimensional stability because of the higher uptake of the liquid electrolyte solution by PAN. However, the polymer blend electrolyte based on 30% PVdF-*co*-HFP–70% PAN is too weak and fragile. Therefore, it cannot be used in practical battery applications because of the PAN-rich phase; it greatly reduces the mechanical strength. Hence, the polymer blend film based on 40% PVdF-*co*-HFP–60% PAN and soaked in a 1*M* $LiClO_4$ electrolyte solution system has been taken as an optimized composition for the preparation of MPGPBEs.

For compatible polymer blends, the glass-transition temperature (T_g) is expected to be intermediate between those of the two polymer components. In the case of the PVdF-*co*-HFP–PAN blend electrolyte, T_g for the polymer component is not observable because the PVdF-*co*-HFP copolymer is semicrystalline, as shown in Figure 2. PVdF-*co*-HFP shows an endothermic peak at 145°C; this can be attributed to the melting of the polymer. On the other hand, increasing the PAN content in the PVdF-*co*-HFP matrix reduces the heat of fusion and lowers the melting temperature (Fig. 2). The depression of the melting point and the reduction of the heat of fusion indicate that PAN is somewhat compatible with PVdF-*co*-HFP. Therefore, increasing the addition of highly amorphous PAN can prevent the crystallization of the PVdF-*co*-HFP copolymer and result in the preservation of amorphous domains, which are responsible for the high affinity to an electrolyte solution. This agrees with the ionic conductivity results.

The crystallinity (X_c) of the PGPBEs was calculated with eq. (3) from the differential scanning calorimetry (DSC) curves[30] (Fig. 2):

$$X_c = (\Delta H_m / \Delta H_m^{\Phi}) \times 100 \quad (3)$$

where ΔH_m^{Φ} is the crystalline melting heat of pure poly(vinylidene fluoride) (104.7 J/g) and ΔH_m is the heat of fusion for PVdF-*co*-HFP–PAN-based blend matrices with different ratios. It can be calculated from the integral area of the baseline and each melting curve. The data for the crystalline melting temperature (T_m), ΔH_m, and X_c are all shown in Table I. Increasing the amount of the PAN polymer slightly influences T_m. However, X_c decreases with an increase in the amount of PAN within the PVdF-*co*-HFP matrix. As a result, it is suggested that the degree of crystallization of the PVdF-*co*-HFP matrix decreases with the addition of PAN. PAN is far

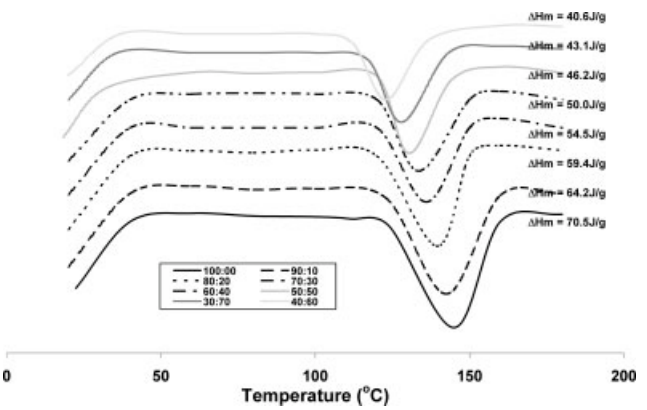

Figure 2 DSC thermograms of PVdF-*co*-HFP–PAN blend electrolytes with different ratios.

TABLE I
T_m, ΔH_m, and X_c Values of PVdF-*co*-HFP–PAN Blend Electrolytes with Different Ratios

PVdF-*co*-HFP:PAN	T_m (°C)	ΔH_m (J/g)	X_c (%)
100 : 0	145.0	70.5	67.33
90 : 10	142.5	64.2	61.31
80 : 20	139.6	59.4	56.73
70 : 30	136.0	54.5	52.05
60 : 40	133.5	50.0	47.75
50 : 50	130.4	46.2	44.12
40 : 60	128.0	40.6	38.77
30 : 70	123.0	43.1	41.16

more respective of the segmental chain motion of the PVdF-*co*-HFP–PAN blend matrix and hence enhances the ionic conductivity.

SEM micrographs for the optimized composition of PVdF-*co*-HFP–PAN-based polymer blend films and microporous polymer blend membranes are shown in Figure 3(a,b). Figure 3(b) shows that much larger voids and cavities of different sizes are due to the skin effect established during the phase-inversion process; more pores are produced in the water-contacting surface than in the surface-contacting surface (glass substrate). The porosity of the membrane was found to be 57.19 ±1.2%. Hence, the uptake of the electrolyte solution by this microporous polymer blend membrane [Fig. 3(b)] is higher than that of plain gel polymer blend film [Fig. 3(a)]. In addition, Figure 4(a,b) shows that ΔH_m of the liquid electrolyte decreases with an increasing quantity of the liquid electrolyte solution by the porous matrix, indicating that porous polymer matrices are more compatible with the liquid electrolyte than nonporous polymer films.

Figure 5(a,b) shows Arrhenius plots of optimized compositions of the PVDF-*co*-HFP–PAN-based PGPBE and MPGPBE. The PGPBE and MPGPBE exhibit different slopes, and this may be attributed to the interaction of the polymer chain segments and liquid electrolyte, which gives the semicrystalline and amorphous structures of the PGPBE and MPGPBE, respectively. Hence, the activation energy of the MPGPBE is lower (14.72 kJ/mol) than that of the PGPBE (24.68 kJ/mol). Furthermore, the ionic conductivity decreases abruptly at a low temperature because the nonsolvent freezes in the gel polymer blend electrolyte and, therefore, the solvent-rich domains of EC exist as crystalline solids at a low temperature. At a higher temperature, the increase in the ionic conductivity is due to inverse ionic mobility; this increase in the amorphous region of the polymer blend results from the increase in the segmental mobility of the polymer chain. This will assist fast ion transport, which may prevent the formation of an ion cloud. However, the polymer chain acquires faster internal modes in which bond rotations produce segmental motions to favor interchain and intrachain ion hoping, and thus the degree of conductivity becomes high.

Figure 6(a,b) illustrates linear sweep voltammetry curves of cells prepared with an optimized composition of a PVDF-*co*-HFP–PAN-based MPGPBE soaked in different electrolyte solutions. From these curves, the difference in the decomposition potentials of two kinds of MPGPBEs arises because of the difference in the electrochemical stability of the electrolyte solutions. Figure 6(b) shows that the $LiAsF_6$-based MPGPBE has current onsets at 5.1 V versus Li/Li^+, and the oxidation current is lower than that of the other system at a higher voltage region; this means

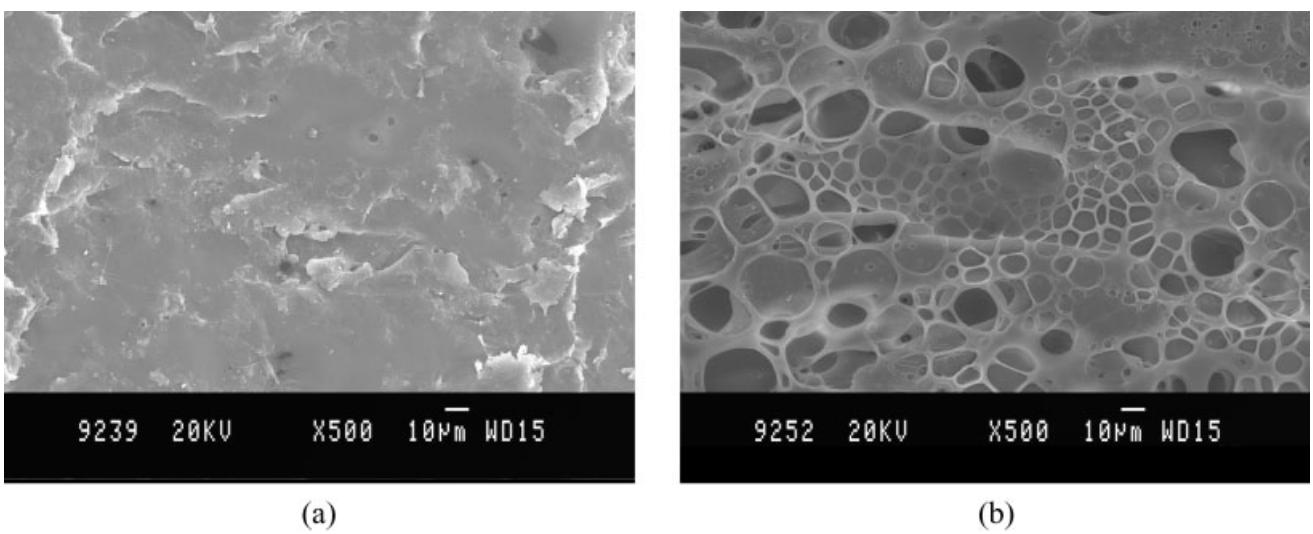

Figure 3 SEM photographs of (a) a plain polymer blend film and (b) a microporous polymer blend membrane based on 40 % PVdF-*co*-HFP–60 % PAN.

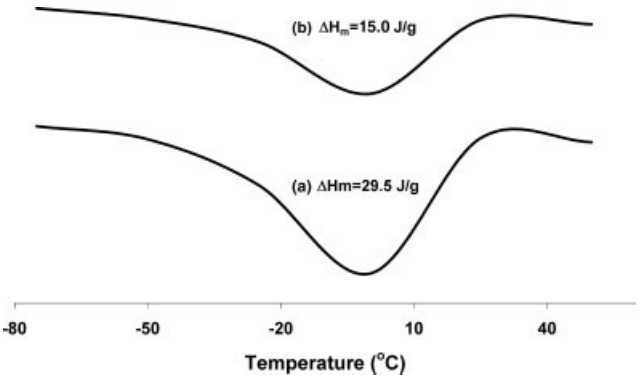

Figure 4 DSC curves of (a) PGPBE and (b) MPGPBE based on 40 % PVdF-*co*-HFP–60 % PAN.

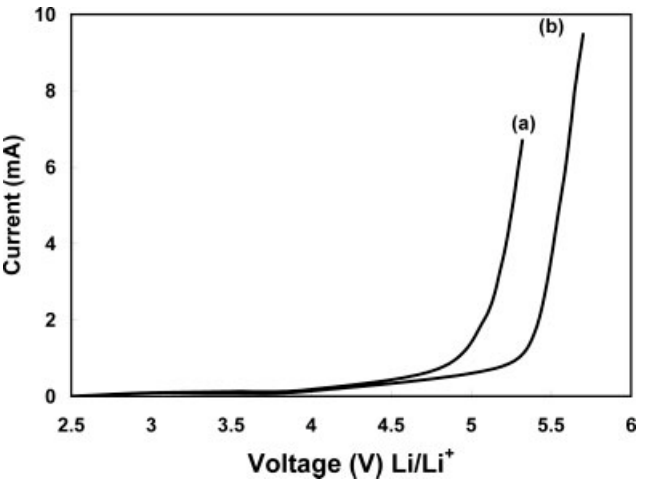

Figure 6 LSV curves of MPGPBEs based on (a) 40 % PVdF-*co*-HFP–60 % PAN–1*M* $LiClO_4$–EC–DEC and (b) 40 % PVdF-*co*-HFP–60 % PAN–1*M* $LiAsF_6$–EC–DEC.

that the MPGPBE prepared through soaking in 1*M* $LiAsF_6$ containing a 1 : 1 (v/v) EC–DEC electrolyte solution is the most resistant to oxidation.

The transference numbers of the optimized composition of the PVDF-*co*-HFP–PAN-based PGPBE and MPGPBE were determined by means of a chronoamperometric technique, as shown in Figure 7(a,b), and the impedance measurements were obtained before and after direct-current polarization measurements with an applied potential difference of 10 mV/s. Figure 7(a) shows that the initial current value (I_0) is 28.21 μA and the steady-state value (I_s) is 17.60 μA within about 2.15 h, and the corresponding alternating-current impedance values, such as the initial resistance of the interface (R_i^0) and steady-state resistance of the interface (R_i^s), are 178.54 and 348.59 Ω, respectively; this gives a transference number of about 0.512. Figure 7(b) shows that I_0 is 26.30 μA and I_s is 18.23 μA within about 1.56 h, and the corresponding alternating-current impedance values, such as R_i^0 and R_i^s, are 142.96 and 210.22 Ω, respectively; this gives a transference number of about 0.680, and the relaxation time of the MPGPBE is much faster than that of the PGPBE. Theoretically, this phenomenon implies that the ionic mobility of the MPGPBE is more facile than that of the PGPBE. Hence, the porous structure present in the polymer film that provides more liquid pathways is probably a positive factor leading to superior ionic transport as well.

The charge–discharge curves of carbon/PGPBE/$LiMg_{0.10}Mn_{1.90}O_4$ and carbon/MPGPBE/$LiMg_{0.10}Mn_{1.90}O_4$ cells are shown in Figure 8(a,b). It is obvious that the cell at the C/10 rate achieves a discharge capacity of 130.0 mAh/g for the MPGPBE. A comparison of the discharge capacities of the MPGPBE and PGPBE shows that the specific capacity of the MPGPBE is higher than that of the PGPBE; this results from the increase in the free volume and amorphousness, which provides mobile Li^+ ions giving rise to the increase in the discharge capacity.

Figure 9 shows the cycle performance of the optimized composition of the PVDF-*co*-HFP–PAN-based

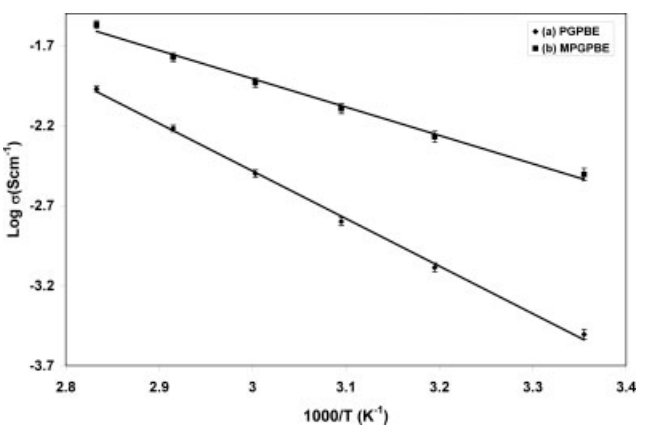

Figure 5 Arrhenius plots of (a) PGPBE and (b) MPGPBE based on 40 % PVdF-*co*-HFP–60 % PAN.

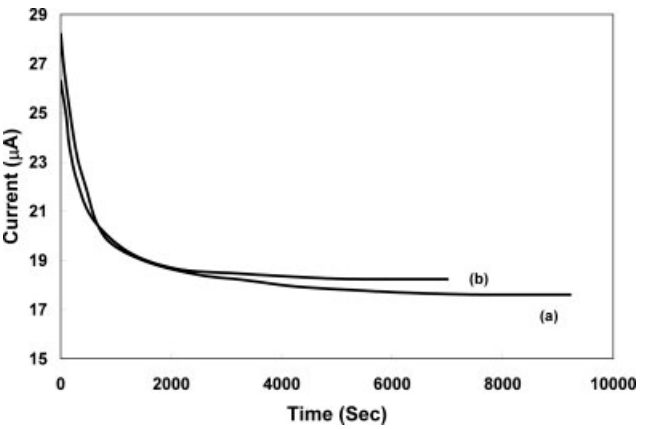

Figure 7 Direct-current polarization curves of (a) PGPBE and (b) MPGPBE based on 40% PVdF-*co*-HFP–60% PAN.

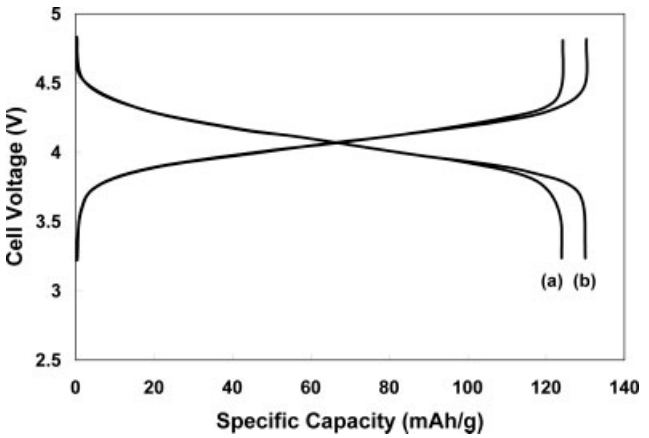

Figure 8 Charge–discharge curves of cells prepared with (a) carbon/PGPBE/$LiMg_{0.10}Mn_{1.90}O_4$ and (b) carbon/MPGPBE/$LiMg_{0.10}Mn_{1.90}O_4$.

PGPBE and MPGPBE. The result shows that the MPGPBE has a more significant effect during the cycle life than the PGPBE. This confirms that the MPGPBE has good compatibility with the electrode materials at the ambient temperature.

The complex permittivity (ε) or dielectric constant of a system is defined as

$$\varepsilon = \varepsilon' - j\varepsilon'' = \varepsilon' - j(\sigma/\omega\varepsilon_0)$$

where ε′ is the real part of the dielectric constant, ε″ is the imaginary part of the dielectric constant of the material, σ is the conductivity, ω is the angular frequency, and ε_0 is the permittivity of the free space. Plots of ε′ verses log *f* for the optimized compositions of the PVDF-*co*-HFP–PAN-based PGPBE and MPGPBE are shown in Figure 10(a,b). The MPGPBE exhibits a much higher ε′ value than the PGPBE at room temperature. The high positive dielectric permittivity obtained in the MPGPBE can be attributed

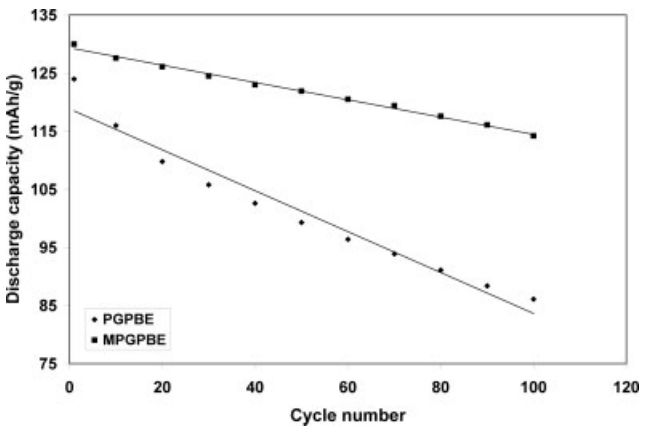

Figure 9 Cycle performance of cells prepared with (a) carbon/PGPBE/$LiMg_{0.10}Mn_{1.90}O_4$ and (b) carbon/MPGPBE/$LiMg_{0.10}Mn_{1.90}O_4$.

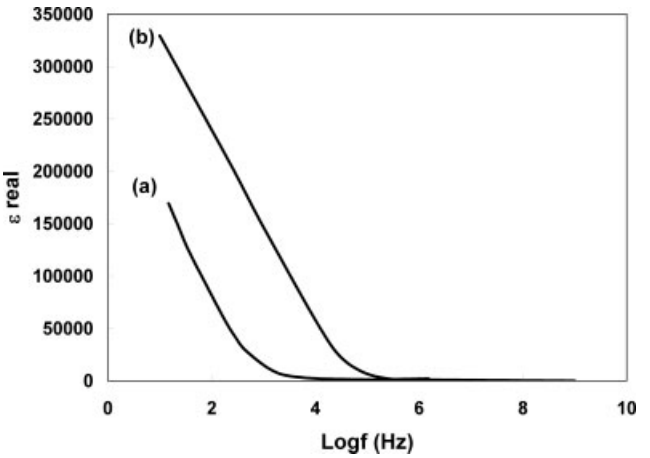

Figure 10 Variation of ε′ as a function of the frequency of cells prepared with (a) SS/PGPBE/SS and (b) SS/MPGPBE/SS.

to the localization of charge carriers. The dielectric permittivity rises sharply toward low frequencies because of electrode polarization effects.[31,32] The low-frequency dispersion region can be attributed to the contribution of charge accumulation at the electrode–electrolyte interface.[33] The high values of ε′ for the MPGPBE system are due to the enhanced charge carrier density in the space charge accumulation region, which results in an increase in the equivalent capacitance. The observed variation in ε′ with the frequency can be attributed to the formation of a space charge region at the electrode–electrolyte interface, which is familiarly known as $w^{(n-1)}$ variation or non-Debye behaviors, in which the space charge regions with respect to the frequency are explained in terms of ion diffusion.[34] At higher frequencies, because of the high periodic reversal of the electric field at the interface, the contribution of charge carriers (ions) toward the dielectric constant decreases with increasing frequency. In addition, the polarization due to charge accumulation decreases, and this results in a decrease in the value of ε′.

CONCLUSIONS

The optimized composition of a PVdF-*co*-HFP–PAN-based MPGPBE was prepared by a phase-inversion technique. The higher ionic conductivity and lithium transference number for the MPGPBE could be attributed to the higher number of effective charge carriers, which was due to the decreased surface/volume ratio of the microporous network, and it also presented stable charge–discharge behavior with little capacity loss. This process is simple and cost-effective for the preparation of MPGPBEs for lithium-ion batteries.

References

1. Tarascon, J. M.; Armand, M. Nature 2001, 414, 359.
2. Scrosati, B.; Croce, F.; Panero, S. J Power Sources 2001, 100, 93.
3. Murata, K.; Izuchi, S.; Yoshihisa, Y. Electrochim Acta 2001, 45, 1501.
4. Brodd, R. J. Interface 1999, 8, 20.
5. Xie, L.; Fouchard, D.; Megahed, S. Proc Mater Res Soc Symp 1995, 393, 285.
6. Scientist Helping America. http://safe.sysplan.com/scihelpamerica/ad.html (accessed 2002).
7. Song, J. Y.; Wang, Y. Y.; Wan, C. C. J Electrochem Soc 2000, 147, 3219.
8. Subramania, A.; Kalyana Sundaram, N. T.; Sukumar, N. J Power Sources 2005, 141, 188.
9. Bruce, P. G.; Vincent, C. A. J Electroanal Chem 1987, 225, 1.
10. Jeon, J. D.; Cho, B. W.; Kwak, S. Y. J Power Sources 2005, 143, 219.
11. Saikia, D.; Kumar, A. Electrochim Acta 2004, 49, 2581.
12. Kim, K. M.; Ko, J. M.; Park, N. G.; Ryu, K. S.; Chang, S. H. Solid State Ionics 2003, 161, 121.
13. Basak, P.; Manorama, S. V. Solid State Ionics 2004, 167, 113.
14. Choi, N. S.; Park, J. K. Electrochim Acta 2001, 46, 1453.
15. Zhu, X. X.; Banana, K.; Liu, H. Y.; Krause, M.; Yang, M. Macromolecules 1999, 32, 277.
16. Zoppi, R. A.; Contant, E. A. R. D. S.; Marques, F. R.; Wada, M. L. F.; Nunes, S. P. Polymer 1999, 40, 3275.
17. Lee, K. H.; Park, J. K.; Kim, W. J. J Polym Sci Part B: Polym Phys 1999, 37, 247.
18. Subramania, A.; Kalyana Sundaram, N. T.; Vijaya Kumar, G. J Power Sources 2006, 153, 177.
19. Tarascon, J. M.; Gozdz, A. S.; Schmutz. C.; Shokoohi, F.; Warren, P. C. Solid State Ionics 1996, 86, 49.
20. Xi, J.; Qiu, A. Solid State Ionics, to appear.
21. Stephan, A. M.; Teeters, D. Electrochim Acta 2003, 48, 2143.
22. He, X.; Shi, Q.; Zhou, X.; Wan, C.; Jiang, C. Electrochim Acta 2005, 510, 1069.
23. Pu, W.; He, X.; Wang, L.; Jiang, C.; Wan, C. J Membr Sci 2006, 272, 11.
24. Pasquier, A. D.; Warren, P. C.; Culver, D.; Gozdz, A. S.; Tarascon, J. M. Solid State Ionics 2000, 135, 249.
25. Magistris, A.; Mustarelli, P.; Parazzoli, F.; Quartarine, E.; Piaggio, P.; Bottino, A. J Power Sources 2001, 97, 657.
26. Manuuel Stephen, A.; Teeters, D. Electrochim Acta 2003, 48, 2143.
27. Magistris, A.; Mustarelli, P.; Quartarone, E.; Piaggio, P. Electrochim Acta 2001, 46 1635.
28. Shi, Q.; Yu, M.; Zhou, X.; Yan, Y.; Wan, C. J Power Sources 2002, 103, 286.
29. Wen, T. C.; Kuo, H. H.; Gopalan, A. Solid State Ionics 2002, 147, 171.
30. Li, Z.; Su, G.; Wang, X.; Gaw, D. Solid State Ionics 2005, 176, 1903.
31. Mishra, R.; Rao, K. J. Solid State Ionics 1998, 106, 113.
32. Campbell, J. A.; Goodwin, A. A.; Simon, G. P. Polymer 2001, 42, 4731.
33. Howell, F. S.; Bose, R. A.; Macedo, P. B.; Moynihan, C. T. J Phys Chem 1974, 78, 639.
34. Impedance Spectroscopy; Macdonald, J. R., Ed.; Wiley: New York, 1987.